NUCLEAR SCIENCE AND ENGINEERING: **133**, 1–22 (1999)

A Liquid-Metal Reactor for Burning Minor Actinides of Spent Light Water Reactor Fuel—I: Neutronics Design Study

Hangbok Choi*

Korea Atomic Energy Research Institute, P.O. Box 105, Yuseong, Taejon, Korea

and

Thomas J. Downar

Purdue University, School of Nuclear Engineering, West Lafayette, Indiana 47907

Received June 5, 1998
Accepted November 24, 1998

Abstract—*A liquid-metal reactor was designed for the primary purpose of burning the minor actinide waste from commercial light water reactors (LWRs). The design was constrained to maintain acceptable safety performance as measured by the burnup reactivity swing, the Doppler constant, and the sodium void worth. Sensitivity studies were performed for homogeneous and decoupled core designs, and a minor actinide burner design was determined to maximize actinide consumption and satisfy safety constraints. One of the principal innovations was the use of two core regions, with a fissile plutonium outer core and an inner core consisting only of minor actinides. The physics studies performed here indicate that a 1200-MW(thermal) core is able to consume the annual minor actinide inventory of about 16 LWRs and still exhibit reasonable safety characteristics.*

I. INTRODUCTION

For the last 40 yr, the utilization of nuclear power has resulted in an accumulation of solidified high-level waste (HLW). The hazard from the HLW can be classified into two sources: fission products and actinides. The short-term hazard is dominated by ^{90}Sr and ^{137}Cs fission products for the first 200 yr. A few other fission products, such as ^{99}Tc and ^{129}I, have very long half-lives; however, the low concentration of these isotopes diminishes their overall importance to the waste hazard. Actinide materials such as ^{241}Am and ^{243}Am have even longer half-lives and dominate the waste hazard beyond 1000 yr. The ^{237}Np isotope has a half-life of 2 million yr, and its hazard dominates up to 20 million yr before the ^{238}U decay chain takes control. In contrast to the current strategy of permanent storage of spent fuel in a geological repository, the transmutation or burning of long-lived actinides by irradiation could be used as a method of ultimate disposal. Earlier studies[1–3] have shown that greater long-term safety could be achieved in the disposal of HLWs if actinides are separated from the fission products and burned in power reactors. If so, the actinides will be continuously recycled and will not be discharged to the environment until the reactor is shut down.

Feasibility studies of actinide transmutation in power reactors have shown that liquid-metal fast breeder reactors (LMFBRs) offer an advantage because of a preferential fission-to-capture reaction ratio in the harder neutron spectrum[4,5] and lower spontaneous fission neutron activity.[6] Research groups at General Electric,[7] Oak Ridge National Laboratory,[8] and Combustion Engineering[9] have studied the actinide transmutation in LMFBRs using specially designed target fuels loaded at the central zone of the core so that the actinides are effectively burned in target zones while the actinide production and destruction are balanced in the rest of the core region at the equilibrium state. Beaman and Aitken[10] used a typical 1200-MW(electric) LMFBR and found that 113 kg of actinides, which is the amount of actinides from one

*E-mail: choih@nanum.kaeri.re.kr

LMFBR and three 1200-MW(electric) light water reactors (LWRs), is burned per cycle. Williams et al.[8] also used a 1200-MW(electric) LMFBR but elevated the specific power and core burnup by 15% from those of a commercial LMFBR. At the equilibrium state, the actinides from one LMFBR and one LWR can be consumed when target fuels are diluted 65% by ^{238}U to prevent local power peaking in the target zone. These studies have shown that the physics characteristics of the system are not sensitive to the actinide target loading.

Robinson et al.[11] proposed a 1100-MW(thermal) actinide burner reactor with a very hard spectrum determined by a sodium-to-fuel ratio of 1.01. Parametric studies were performed for core geometry (homogeneous and two-zone core), fuel composition, lattice arrangement, actinide fuel type, and the concentration of molybdenum diluent. This conceptual burner model could process two conventional 1100-MW(electric) LWRs when optimized in a two-zone reactor. Balz et al.[12] have studied minor actinide burning in the European fast reactor. Parametric studies on the minor actinide content showed that the void worth increased too much when the minor actinide content exceeded 10% because the reactivity worth of ^{237}Np and ^{241}Am increases much more than the worth of ^{238}U upon core voiding. On the other hand, the Doppler constant decreased too much when the minor actinide content exceeded the limiting value because resonance capture of ^{237}Np and ^{241}Am is less sensitive to temperature change than that of ^{238}U, which is the most dominant resonance absorption isotope in the commercial power plant. Because of limitations on the minor actinide content, the core design of Balz et al. can consume the minor actinide inventory of only four LWRs of the 1200-MW(electric) type.

Japanese research groups are actively involved in transmutation analysis of minor actinides in fast reactor systems. Wakabayashi et al.[13] have studied a 1000-MW(electric) LMFBR with a homogeneous loading of transuranic (TRU) nuclides. In the case of oxide fuel, the amount of TRU from six 1000-MW(electric) LWRs, which is 5% of the total heavy-metal loading, can be transmuted without any degradation of core performance. Hayase et al.[14] have used mixed oxide fuel with a 10% enrichment of minor actinides in a 1000-MW(electric) LMFBR. They could dispose of minor actinides from ten 1000-MW(electric) LWRs per year with a 35% increase in the sodium void worth as a penalty compared to the core without minor actinide enrichment.

There has also been considerable research on metallic fuels because of the benefits of the harder neutron spectrum as well as the possibility of a more compact and economical fuel cycle. Mukaiyama et al.[15] have designed a minor actinide burner (MAB) with two alloy fuels: Np-(Pu)-Zr and Am-Cm-(Pu)-Y. This MAB can burn the minor actinides from 12 typical 1000-MW(electric) LWRs. Sasahara and Matsumura[16] have also used metallic fuel in a 1000-MW(electric) LMFBR. Their core design consisted of two homogeneous zones; the plutonium enrichment is higher in the outer core to control the reactivity and power distribution. Their metal fuel burner is capable of transmuting TRUs produced from eighteen 1200-MW(electric) LWRs. Hill et al.[17] have applied the integral fast reactor[18] (IFR) concept to a 1200-MW(thermal) MAB design that was modeled homogeneously after a small change of fuel pin size. This MAB could burn the minor actinides of twelve 1000-MW(electric) LWRs. A similar study[19] by Rockwell International used a two-zone core concept for a 1160-MW(thermal) MAB. This MAB could burn minor actinides of fifteen 1000-MW(electric) LWRs, but the sodium void worth and reactivity burnup swing were estimated to be much higher than those of Hill et al.'s design.

The objective of this work is then to perform physics studies of an MAB design with a minor actinide inventory much greater than would be considered to be practical with current nuclear fuel technology and to determine if an acceptable core safety performance can be achieved. Specifically, this study will examine three of the most important safety performance parameters of a liquid-metal reactor (LMR): the burnup reactivity swing, the sodium void worth, and the Doppler constant.

II. DESIGN MORPHOLOGY

II.A. Design Criteria

The neutronics design of a reactor core needs data from thermal-hydraulics and material analysis. Because the properties of minor actinide fuels and the characteristics of the fuel assembly are not known at the beginning of design analysis, some of these parameters have to be assumed based on similar core designs. The sodium advanced fast reactor[20] (SAFR) and Japanese actinide burning reactor[21] (ABR) core models supply reasonable initial design data. The nominal design is the same as the IFR core, which is the updated version of the SAFR core: 91.44 cm (36 in.) of active fuel height, 0.724 cm (0.285 in.) of pin diameter, and 900 MW(thermal) of reactor power. These parameters are to change, depending on the performance of the MAB.

The fuel is composed of actinide material and 25% of zirconium. The theoretical density is assumed to be 75% to allow for fuel expansion and a high discharge burnup.[20] The fuel does not have an axial blanket in order to simplify the fabrication process. The design limit of the discharge burnup is 200 MWd/kg. There is no design limit for burnup reactivity swing and coolant void worth. But, the absolute value of the burnup reactivity swing and the coolant void worth should be as small as possible, satisfying other design limits. In this study, these are tentatively assumed to be $\pm 1\%\ \delta k$. The thermal conductivity of minor actinide alloy fuel is expected to be smaller than that of U-Pu-Zr alloy.[21] Comparing the values

used for the SAFR and ABR designs, the thermal conductivity of 22 W/m·K is used for minor actinide alloy fuel. It is assumed that the pumping power is enough to maintain a coolant velocity of 6 m/s.

The most crucial design criterion is the peak linear power because the fuel centerline temperature cannot exceed the melting point (1160°C). The design limit of peak linear power for the IFR is 49.2 kW/m, but the peak power density of IFR fuel (40.0 kW/m) is used here for the regular fuel pins in the MAB design to allow more thermal margin. The nominal design data and design limits are summarized in Table I.

II.B. Cross-Section Data

The diffusion and depletion codes used in the work are DIF3D (Ref. 22) and REBUS-3 (Ref. 23), respectively, which require the cross-section data in the format of ISOTXS. Argonne National Laboratory research groups have generated a 9-group ISOTXS set by processing ENDF/B-V for the analysis of an LMR such as the SAFR and the IFR cores. This 9-group cross-section set was used for all depletion calculations of the MAB conceptual design, as was done by the other study.[17] In addition, three 21-group cross-section sets were also generated to evaluate the void worth and Doppler constant for different reactor conditions such as flooded, voided, and hot core. The flooded core has normal temperatures and coolant densities. In the voided core, the coolant that directly comes into contact with the fuel rods is voided in the active core, upper plenum, and upper shield region. The coolant in the duct region and the nonfuel channel is assumed not to be voided because the voiding in these low-power regions is expected to be delayed compared with the fuel assembly. The hot core cross-section data were prepared by doubling the fuel temperature.

TABLE I

Nominal Design Parameters of MAB

Reactor power [MW(thermal)]	900
Active core height (cm)	91.44
Fuel design	
Material type	MA/Pu + 25% Zr alloy
Theoretical density (%)	75
Discharge burnup (MWd/kg)	200
Cooling time (yr)	
LWR-discharged fuel	3
MAB-discharged fuel	2
Reprocessing time (month)	6
Refabrication time (month)	6
Recovery factors	
U/Pu/MA	1.00
Americium and fission product	0.04

II.C. Fuel Cycle Model

In the MAB, it is important to "close" the fuel cycle such that the minor actinides are not discharged to the environment throughout the reactor lifetime. Because the reprocessing and fabrication of minor actinide fuel has not been developed and demonstrated precisely, the following fuel cycle scenario is tentatively used for the MAB fuel cycle.

II.C.1. In-Core Fuel Cycle

It is practical to assume that a reactor is operated on a fixed fuel management scheme and maintains its criticality during normal operation. Under these conditions, the reactor condition is invariant for successive fuel cycles, and this core is called a *k*-constrained equilibrium core. The core can also be constrained with the discharge burnup, but only the *k*-constraint was used in the MAB design. The equilibrium core is found by adjusting the charge enrichment, which is defined as the volume ratio of class 1 to class (1+2) fuels. Typically, class 1 is defined as the more reactive materials by the users. The following equations describe the solution strategy:

$$\vec{N}_r = \boldsymbol{M}(T, e, \vec{N}_C)\vec{N}_C \ , \tag{1}$$

$$\vec{N}_C = \boldsymbol{Q}_r(\vec{N}_r)\vec{N}_r + \boldsymbol{Q}_f(\vec{N}_r)\vec{N}_f \ , \tag{2}$$

and

$$k = k(T, e, \vec{N}_C) \ . \tag{3}$$

In Eq. (1), the discharge number density vector $\vec{N}_r$ is determined by the transmutation matrix $\boldsymbol{M}$ and initial number density vector $\vec{N}_C$. The transmutation matrix is expressed as a function of cycle length T, charge enrichment e, and charge density. Because the cross section is an invariant quantity and the transmutation flux is a function of cross section and number density, they are not shown in Eq. (1). After each cycle, the charge density is re-calculated using the discharge density and external feed density $\vec{N}_f$ in Eq. (2). The discharged fuel is reprocessed and shuffled through the operator $\boldsymbol{Q}_r$. The external feed material, which is LWR-discharged fuel in this study, is processed through the fabrication operator $\boldsymbol{Q}_f$. If the *k*-constraint—which is expressed as a function of cycle length, charge enrichment, and charge density in Eq. (3)—is not satisfied either at the beginning-of-equilibrium-cycle (BOEC) or end-of-equilibrium-cycle (EOEC) state, the region-dependent charge density e is linearly interpolated based on the previous estimate. The new charge density is calculated using the compositions of class 1 and 2 feed material obtained from Eq. (2). These procedures are continued until the constraint is satisfied and number densities are converged.

II.C.2. Ex-Core Fuel Cycle

The MAB has two fuel sources: LWR- and MAB-discharged fuel. The LWR-discharged fuels are sent to

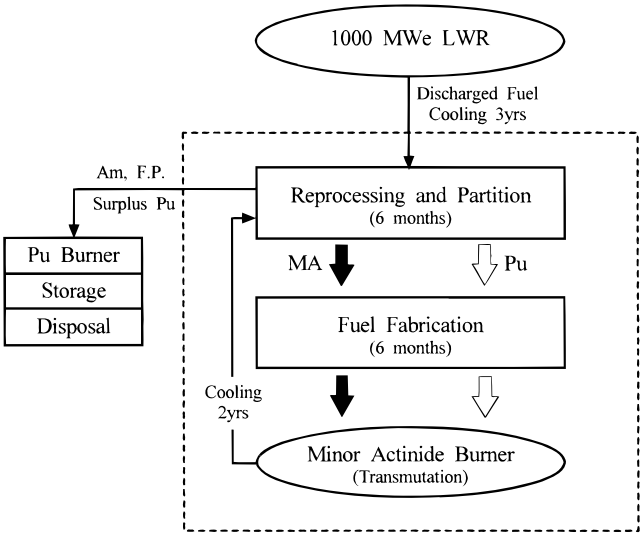

Fig. 1. Mass flow of MAB fuel cycle.

TABLE II

Isotopic Composition of Discharged Fuel from 1000-MW(electric) LWR After 3 yr of Cooling

Class 1[a]		Class 2[b]	
^{236}Pu	1.26×10^{-7}	^{237}Np	0.491
^{238}Pu	1.14×10^{-2}	^{241}Am	0.227
^{239}Pu	0.571	^{242m}Am	1.00×10^{-3}
^{240}Pu	0.224	^{243}Am	0.225
^{241}Pu	0.151	^{242}Cm	8.81×10^{-5}
^{242}Pu	4.36×10^{-2}	^{243}Cm	7.12×10^{-4}
		^{244}Cm	5.00×10^{-2}
		^{245}Cm	4.60×10^{-3}
		^{246}Cm	5.72×10^{-4}

[a]Class 1 is the more reactive isotope group.
[b]Class 2 is the less reactive isotope group.

the pyrochemical plant after a 3-yr cooling time and reprocessed with MAB-discharged fuels that have been cooled for 2 yr. In the pyroprocess, plutonium and uranium are collected on the cathodes with minor actinides.[24] Fission products and americium are not separated in this process and are sent to storage. But, the recovery factors of fission products and americium are assumed to be 4%, based on Ref. 25, to allow for possible impurities during the reprocessing, and further partitioning of minor actinides (e.g., ^{237}Np) is assumed to be done in the second stage of the pyroprocess (postreprocess). Total reprocessing time is assumed to be 6 months. After reprocessing, fuels are fabricated in the fabrication plant, and excess plutonium will be sent to a plutonium-burning core or to a storage facility. Therefore, minor actinides, except americium, which is not recovered in the pyroprocessing, are enclosed in a fuel cycle that is composed of an MAB and a reprocessing plant. The fabrication time is assumed to be 6 months. The overall mass flow is depicted in Fig. 1. The isotopic composition of a typical LWR-discharged fuel is shown in Table II.

II.D. Safety Performance Parameters

II.D.1. Burnup Reactivity Swing

The burnup reactivity swing is defined as the difference of unpoisoned k_{eff} at the BOEC and EOEC states ($\delta k_{BU} = k_{\mathrm{BOEC}} - k_{\mathrm{EOEC}}$). The unpoisoned k_{eff} is the effective multiplication factor when the core does not have poison material such as burnable poison or control rods. It is desirable to minimize the $|\delta k_{BU}|$ because consequences of the control rod runout transient overpower (TOP) event can be minimized[26] with near-zero δk_{BU}. If the core geometry and other parameters are fixed, the burnup swing depends on cycle length and fuel composition. The $|\delta k_{BU}|$ increases as the cycle length increases because the fissile material is destroyed or bred continuously during the fuel cycle. It is possible to reduce $|\delta k_{BU}|$ using a relatively short cycle length, but this requires frequent reactor shutdown for refueling, and the fuel economy becomes poor because of low discharge burnup. This problem can be resolved to a certain extent by incorporating a multibatch core model that has an appropriate cycle length and number of batches.

II.D.2. Sodium Void Worth

The loss of sodium has a global effect of positive reactivity in most LMR cores because of several mechanisms[27]: spectral hardening, reduction in sodium capture, and change in self-shielding. If the sodium is lost, the neutron moderation is reduced, and the spectrum hardens. The spectral hardening is the most dominant effect of positive void worth. If the coolant is voided, the neutrons have a greater probability to escape the core, and this results in the negative effect on the void worth. Hitachi[28] proposed a core that is loaded with partial fuel on the upper boundary area such that the δD increases considerably on the boundary in the case of coolant voiding. The pancake-type core has a large flux gradient, and the void worth could be negative if the ratio of height to diameter (H/D) is very small[29] ($\sim$0.2). But, the neutron economy of a high-leaking core is poor and requires more fissile material to compensate for the neutron losses. Therefore, the burnup reactivity swing would be increased, and the minor actinide transmutation will be reduced. The design options that can reduce the void worth will have trade-offs for other performance parameters such as the burnup reactivity swing and minor actinide transmutation.

II.D.3. Doppler Constant K_D

The Doppler constant is defined as the change in reactivity due to the relative variation of fuel temperature. The reactivity changes because the capture and fission resonances are broadened as the temperature increases (Doppler effect). In a typical fast reactor, the absorption in the region of well-separated resonances is much smaller compared to a thermal reactor because the neutron spectrum is harder and the resonance peaks become flatter at higher neutron energy.[30] Because of the harder spectrum and the nature of resonances at high energy, the Doppler effect is dominant in the region of ~1 keV. It is important to keep the Doppler constant negative to have a prompt negative feedback from the prompt critical core in the case of a power transient because the control rod movement is slow after a prompt critical excursion. A relatively large part of the Doppler effect comes from fertile material, ^{238}U or ^{232}Th, because of their large increase in the effective parasitic capture cross sections. In the MAB design, ^{238}U is not fed to the core to prevent further higher actinide production. Because metallic fuel is used in the MAB, the spectrum is even harder, and the magnitude of the Doppler constant will be very small. As far as the Doppler constant is concerned in this study, a core model with a negative Doppler constant will be accepted regardless of its magnitude.

III. HOMOGENEOUS MINOR ACTINIDE BURNER DESIGN

The presence of a substantial minor actinide inventory in the fuel poses some challenging core design problems. For example, the buildup of the highly reactive ^{238}Pu from neutron capture in ^{237}Np makes it difficult to maintain both a low burnup reactivity swing and a low sodium void worth. The effort to minimize the buildup of more TRU isotopes during core operation discourages the use of fertile material[31] such as ^{238}U, and this causes a very small Doppler constant.

The homogeneous core model is preferable because it simplifies fuel fabrication and management. However, the void worth of homogeneous cores becomes unacceptably large (positive) as the minor actinide inventory is increased because of the fast fission effect of the minor actinides (e.g., ^{237}Np). On the other hand, if the fuel volume fraction is reduced to increase the core leakage and reduce the void worth, the burnup reactivity swing becomes unacceptably large, and the minor actinide inventory is reduced. In general, the most important performance parameters (burnup reactivity swing, sodium void worth, and Doppler constant) cannot be satisfied completely because the design changes that favor one parameter generally have a deleterious effect on the others.[32]

In Secs. III.A through III.F the assumptions used in the MAB fuel cycle are discussed, and a parametric study is performed for homogeneous core models. A homogeneous core was selected first as a base model for the MAB design. The cycle length was studied to see the effect on the burnup reactivity swing. Fuel assembly design was studied by changing the pitch length and number of fuel pins. The effect of reactor power was studied too, and finally, the core geometry was altered to the pancake core and annular model.

III.A. Base Minor Actinide Burner Model

As a first step, the MAB core was modeled homogeneously. To simplify the fuel fabrication, we did not consider axial or internal blankets. The base core model was selected based on the IFR fuel design with a reactor power of 900 MW(thermal). Several B_4C blocks were deployed to reduce the possible power peaking in the central zone. The horizontal and vertical configurations of the base core model are shown in Figs. 2 and 3, respectively. The radial boundary of the core is reflected and shielded with stainless steel and B_4C blocks, respectively. The fuel assemblies have an active core height of 91.44 cm with a 15.4758-cm lattice pitch in the hexagonal array. In the fuel assemblies, a 30.48-cm-thick lower axial shield is placed below a 50.8-cm-thick lower plenum zone. Above the active core, there is a 127-cm-thick upper plenum and a 30.48-cm-thick axial shield. The plenum region is composed of sodium coolant and HT-9 structural material. The axial shield zone is filled with

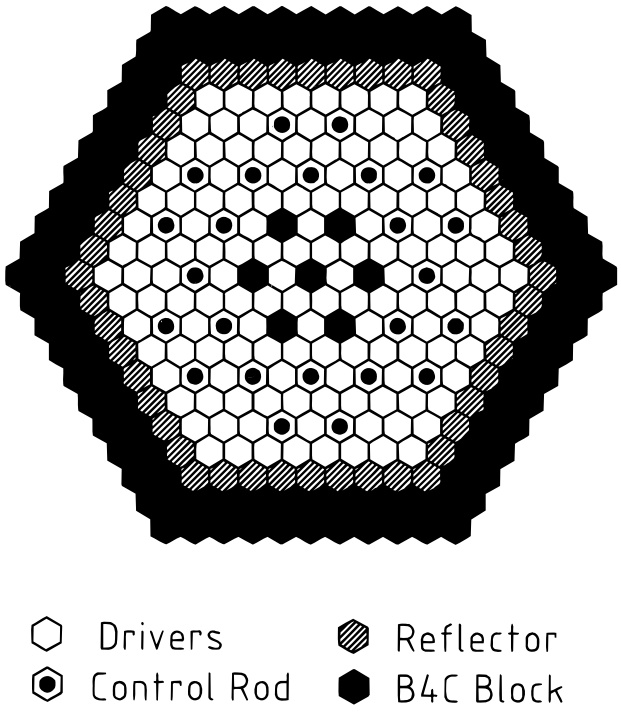

Fig. 2. Horizontal view of homogeneous base core.

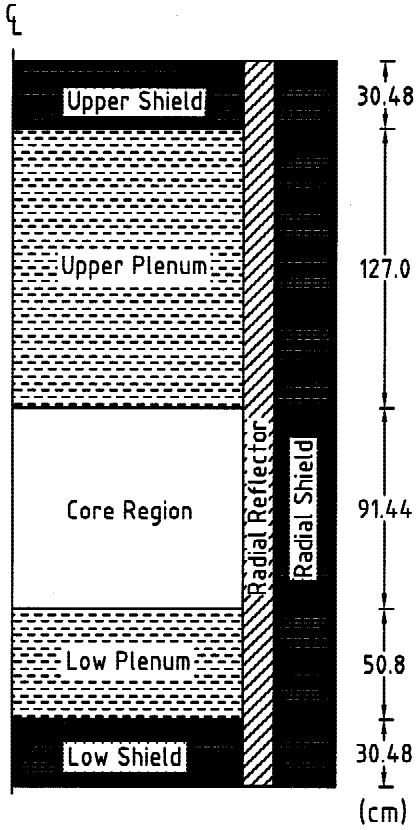

Fig. 3. Vertical view of homogeneous base core.

the coolant, structural material, and B_4C absorber. The absorbing parts of the control assemblies are parked above the active core. The characteristics of the base core are given in Table III.

The charged fuel of the base core is composed of 90% minor actinides, and a total of 877 kg of minor actinides is accepted as an external feed from LWR-discharged fuel every year. However, because of the restriction imposed on the recovery factor, 347 kg of americium is not enclosed in the fuel cycle, and the net annual minor actinide consumption rate becomes 531 kg/yr. The most abundant material (40 wt% of charged fuel) in the core is ^{237}Np, which through neutron capture becomes ^{238}Pu, which is very reactive in a hard neutron spectrum. For example, the η's of ^{237}Np and ^{238}Pu are 0.94 and 2.46, respectively, in this system. Therefore, the transmutation of ^{237}Np and production of ^{238}Pu lead to a negative burnup swing (e.g., the core reactivity increases during the burnup cycle). The void worth is large and positive because most of the minor actinides have a fast fission cross section at a higher-energy region >1 MeV. Most of the positive effect comes from the increased fast fission (due to spectrum hardening) of ^{237}Np, which is most abundant in the base core. The leakage component is 5% of the total worth of the absolute value at BOEC.

TABLE III

Characteristics of Homogeneous Base Core

Reactor concept	Homogeneous
Reactor power [MW(thermal)]	900
Active core height (cm)	91.44
Number of drivers	138
Number of control rod site	24
Number of B_4C block	7
Fuel cycle	
Capacity factor (%)	80
Cycle length (days)	304
Fuel residence time (batch)	2
Fuel data	
Mass ratio (U/Pu/Np/Am/Cm)	4/5/72/11/8
Fuel pin outer diameter (cm)	0.724
Clad thickness (cm)	0.056

The void worth at EOEC is somewhat smaller because 11% of the minor actinides is transmuted at the discharged state. In this study, the void worth and Doppler constant were evaluated only at the BOEC state for the homogeneous core models. The Doppler constant is very small at BOEC ($K_D = -9.4 \times 10^{-5} T\delta k/\delta T$) and does not change much during the cycle. Because there is no strong resonance material, the Doppler effect comes from the most abundant material ^{237}Np, which has its highest resolved resonance at 130 eV. The properties of the base core are summarized in Table IV.

TABLE IV

Properties of Homogeneous Base Core

Minor actinide external feed (kg/yr)	877
Burnup reactivity swing (% δk)	−2.1
Breeding ratio	1.18
Discharge burnup (MWd/kg)	67
Peak linear power (kW/m)	40.3
Peak flux (10^{15} n/cm$^2\cdot$s)	3.5
Peak fast flux (10^{15} n/cm$^2\cdot$s)	2.8
Charge enrichment (wt%)	
Minor actinide	90.3
Fissile plutonium	0.3
Coolant void worth (% δk)	
BOEC	4.1
EOEC	4.0
Doppler constant ($10^{-4} T\delta k/\delta T$)	
BOEC	−0.94
EOEC	−0.94

III.B. Effect of Fuel Cycle Length

The base core was run with two cycle lengths—304 and 608 days—using a one-batch mode in which all the fuel is charged and discharged at the same time. Because the fuel residence time of the long cycle (608 days) is twice that of a short cycle (304 days), the minor actinide transmutation of the long cycle is almost twice that of the short cycle at the discharged state (EOEC). But, the annual minor actinide consumption is only 2% higher in the short-cycle model compared to the long-cycle model. The burnup reactivity swing is much higher in magnitude for the long-cycle model because more ^{238}Pu is produced during the cycle.

The minor actinide consumption of the base core model, which has two batches, is slightly (~1%) higher than that of the short-cycle model. And, the burnup reactivity swing of the base core is almost the same as that of the short-cycle model. The void worth and Doppler constant of these three models are close to each other. For the short-cycle model with a single batch, the fuel fabrication effort will be doubled because all fuel assemblies are charged at the BOEC state, while only half of the fuel assemblies are newly loaded in the base core model. Therefore, the multibatch core with the shorter cycle length has an advantage in burnup reactivity swing and fabrication cost reduction if the cycle length is not too short. The effect of the cycle length is summarized in Table V.

III.C. Effect of Sodium Fraction and Core Size

III.C.1. Sodium Fraction

There are 271 fuel pins in the base core fuel assembly. The numbers of fuel pins were changed to 217, 169, and 91, which correspond to the pin pitch lengths of 0.960, 1.097, and 1.537 cm. The core volume was increased radially (Figs. 4, 5, and 6) as the pitch length increased to conserve the total fuel volume, and therefore, the larger core has a larger sodium fraction. Other fuel cycle parameters are the same as the base core model. The increasing sodium fraction causes spectrum softening, as shown in Fig. 7 (the mean neutron energy decreases from 715 to 699, 666, and 592 as the number of fuel pins changes to 217, 169, and 91, respectively), and more neutron leakage. As the spectrum becomes softened, the core needs more fissile material to maintain the excess reactivity. Because of a lower minor actinide charge enrichment and softer spectrum, the minor actinide consumption is considerably deteriorated in the core with a large sodium fraction. The burnup reactivity swing changes from −2.1 to 2.8% δk as the sodium fraction changes from 0.36 to 0.73 because more fissile material is loaded as the sodium fraction increases.

The void worth increases as the sodium fraction increases up to ~0.6 and then decreases. The spectral and leakage component are proportional to the magnitude of the void perturbation and flux level. Because the variation of the perturbation and flux level is not a linear function of the sodium fraction, the void worth increases in the undermoderated region and decreases in the overmoderated region, which leaves a void worth peak at the

TABLE V

Effect of Cycle Length

	BASE	CY304[a]	CY608[b]
Power [MW(thermal)]	900	900	900
Cycle length (day)	304	304	608
Number of batches	2	1	1
Number of drivers	138	138	138
Actinide consumption (kg/yr)			
Fissile plutonium	−12	−12	−13
Total plutonium	−252	−246	−238
Minor actinide	531	526	518
Reactivity worth (BOEC)			
Burnup swing (% δk)	−2.1	−2.0	−3.8
Void worth (% δk)	4.1	4.2	4.2
Doppler ($10^{-4}T\delta k/\delta T$)	−0.94	−0.92	−0.91

[a]Cycle length equals 304 days.
[b]Cycle length equals 608 days.

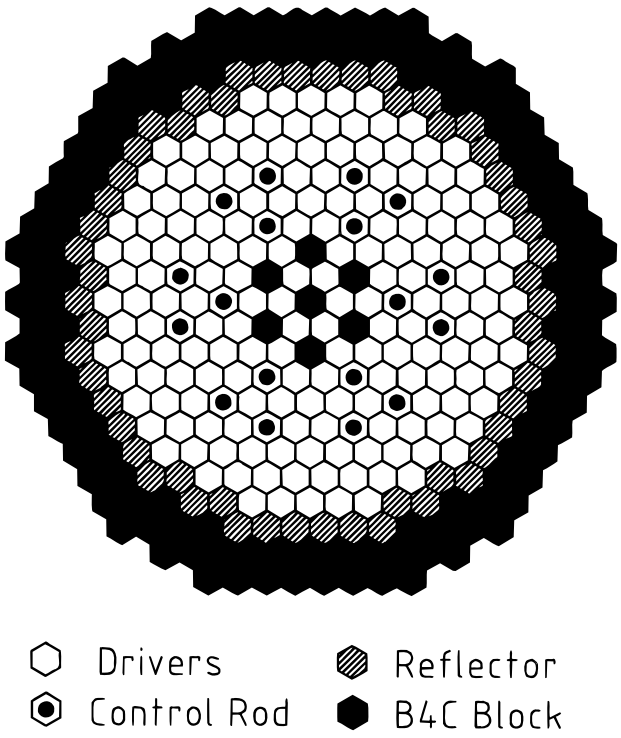

Fig. 4. Homogeneous core model with a sodium fraction of 0.469.

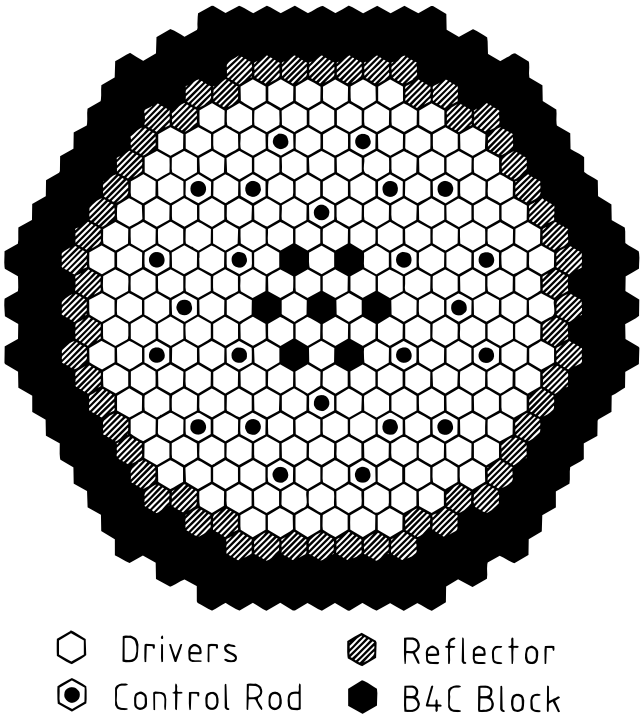

Fig. 5. Homogeneous core model with a sodium fraction of 0.567.

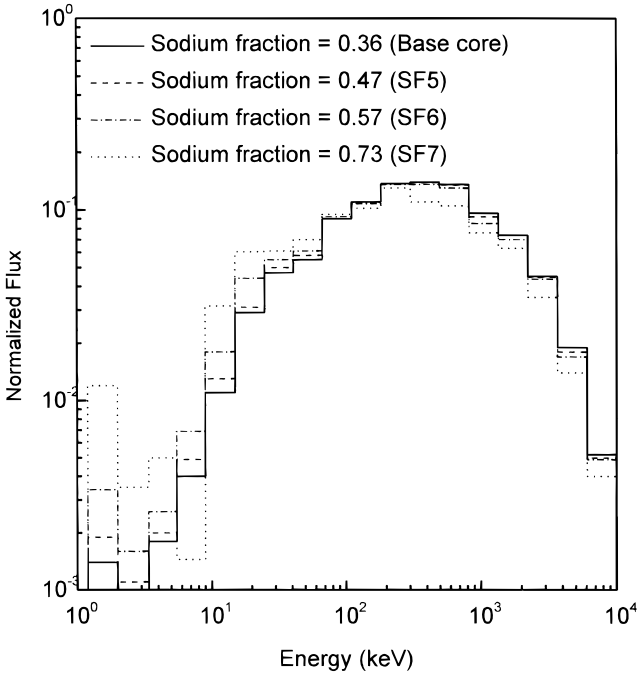

Fig. 7. Spectrum softening due to sodium fraction.

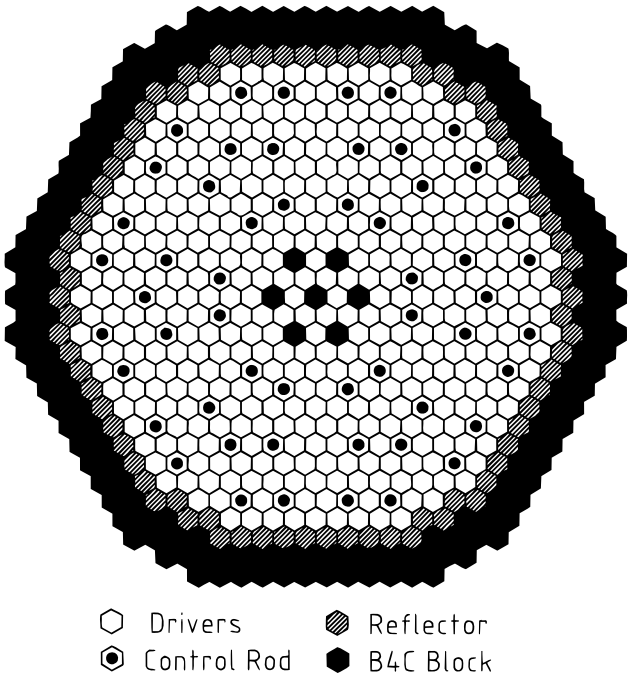

Fig. 6. Homogeneous core model with a sodium fraction of 0.727.

intermediate region, as sodium fraction increases. The negative effect of the leakage component does not decrease the void worth until the assembly is mostly composed of sodium (~70%) such that the axial leakage becomes dominant through both the voided channel and upper plenum.

As the spectrum shifts to the epithermal region, the Doppler effect becomes large. The Doppler constant for a high-sodium-fraction (0.73) assembly is ~2.7 times larger $(-2.4 \times 10^{-4} T\delta k/\delta T)$ than that of the base core $(-9.4 \times 10^{-5} T\delta k/\delta T)$ in absolute value. The fuel composition also contributes to the Doppler constant. Plutonium-240, which has a large resonance at 2.4 keV, comprises 22.9% of the charge density for the core with a sodium fraction of 0.73, while it is only 0.75% for the base core. The effect of the sodium fraction is summarized in Table VI.

III.C.2. Core Size for High-Sodium-Fraction Assembly

The core with a high sodium fraction (0.73) has 390 driver assemblies. This core was studied more closely to examine the effect of core size on neutron leakage. The reactor power was the same as the base core model [900 MW(thermal)], but the number of driver assemblies was reduced to 294 and 222. Because the same reactor power was used, the linear power and discharge burnup increased as the fuel inventory was reduced. It was assumed that the fuel pin could be split into smaller pins to

TABLE VI

Effect of Sodium Fraction

	BASE	SF5[a]	SF6[b]	SF7[c]
Power [MW(thermal)]	900	900	900	900
Cycle length (day)	304	304	304	304
Number of batches	2	2	2	2
Number of drivers	138	174	222	390
Fuel pin pitch (cm)	0.853	0.960	1.097	1.537
Fuel pins per assembly	271	217	169	91
Fuel fraction (100% theoretical density)	0.385	0.308	0.240	0.129
Structure fraction	0.256	0.223	0.193	0.144
Sodium fraction	0.359	0.469	0.567	0.727
Actinide consumption (kg/yr)				
Fissile plutonium	−12	−14	−13	117
Total plutonium	−252	−226	−113	162
Minor actinide	531	505	394	133
Reactivity worth (BOEC)				
Burnup swing (% δk)	−2.1	−1.7	−0.4	2.8
Void worth (% δk)	4.1	6.1	7.3	3.3
Doppler ($10^{-4}T\delta k/\delta T$)	−0.94	−0.98	−0.50	−2.40

[a]Sodium fraction equals 0.469.
[b]Sodium fraction equals 0.567.
[c]Sodium fraction equals 0.727.

reduce the fuel centerline temperature if the peak linear power exceeded the design limit.

Because the reactor power is the same, the peak fast flux of the 222-driver core is 1.6 times higher than that of the 390-driver core. Therefore, the neutron leakage is high in the smaller core because of core size and flux level, and the reactivity loss is compensated for by the high fissile charge enrichment. Because the fissile inventory is large (~36 wt%), the burnup reactivity swing is very high (7.1% δk), but the negative void worth was achieved at BOEC of the small core. The minor actinide consumption is poor in the small core because the core is mostly fed with plutonium. The characteristics of the small cores are compared in Table VII.

III.D. Effect of Moderating Material

One way to prevent spectrum hardening is to use scattering rods such that the neutron is still moderated even if the sodium is lost. The fuel assembly of a 390-driver core (Fig. 6) was modified such that it contains 91 fuel pins and 180 BeO rods. The BeO rod has the same size as a regular fuel pin, and therefore, the coolant area of the moderated assembly is the same as that of the base core assembly. In the 390-driver core, the replacement of BeO rods with sodium induced more spectrum softening, as shown in Fig. 8 (reducing the neutron mean energy to 504 keV), and therefore, minor actinide consumption deteriorated. Though the burnup reactivity swing was increased by 0.56% δk from the unmoderated core (390-driver core without BeO rods), the sodium void worth was reduced to 0.53% δk at BOEC because the scattering cross section was not perturbed much because

TABLE VII

Effect of Core Size for High Sodium Fraction (0.727) Core

	SF7[a]	SF7M[b]	SF7S[c]
Power [MW(thermal)]	900	900	900
Cycle length (day)	304	304	304
Number of batches	2	2	2
Number of drivers	390	294	222
Actinide consumption (kg/yr)			
Fissile plutonium	117	144	192
Total plutonium	162	200	267
Minor actinide	133	95	31
Reactivity worth (BOEC)			
Burnup swing (% δk)	2.8	4.4	7.1
Void worth (% δk)	3.3	1.5	−2.0
Doppler ($10^{-4}T\delta k/\delta T$)	−2.4	−3.4	−6.1

[a]Sodium fraction equals 0.727.
[b]Sodium fraction equals 0.727, medium core.
[c]Sodium fraction equals 0.727, small core.

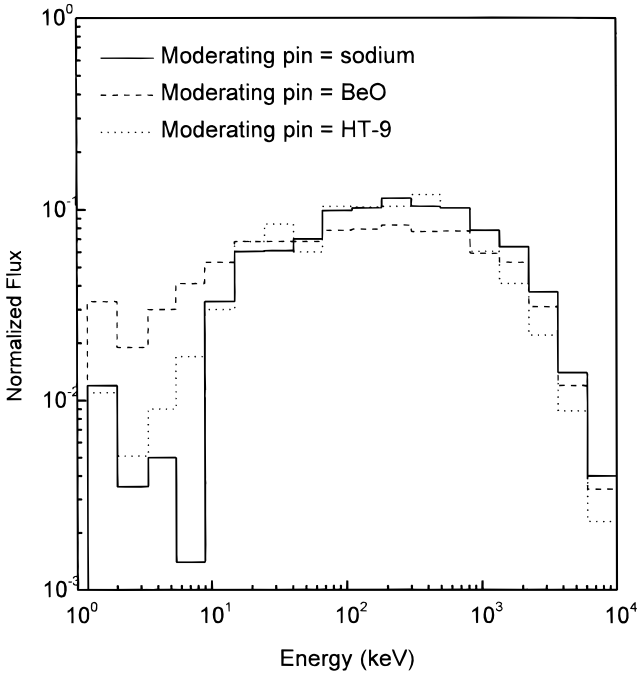

Fig. 8. Spectrum softening due to moderating pins.

TABLE VIII

Effect of Moderating Pins*

	SF7[a]	SF7BE[b]	SF7HT[c]
Power [MW(thermal)]	900	900	900
Cycle length (day)	304	304	304
Number of batches	2	2	2
Number of drivers	390	390	390
Moderating material	–––	BeO	HT-9
Actinide consumption (kg/yr)			
Fissile plutonium	117	169	167
Total plutonium	162	235	232
Minor actinide	133	67	68
Reactivity worth (BOEC)			
Burnup swing (% δk)	2.8	3.4	3.9
Void worth (% δk)	3.3	0.5	0.2
Doppler ($10^{-3}T\delta k/\delta T$)	−2.4	−3.9	−0.5

*Ninety-one regular fuel pins plus 180 moderating pins per assembly.

[a]Sodium fraction equals 0.727.

[b]Sodium fraction equals 0.727, moderated by BeO.

[c]Sodium fraction equals 0.727, moderated by HT-9.

of the scattering rods. If the HT-9 is used as a moderating material in the same core model, the mean neutron energy drops to 465 keV, and it was possible to reduce the void worth to 0.22% δk at BOEC, but there were tradeoffs in minor actinide consumption and burnup reactivity swing. The effect of scattering material is summarized in Table VIII.

III.E. Effect of Reactor Power

Instead of changing reactor size, the reactor power was reduced to 600 and 330 MW(thermal), for which the numbers of drivers are 102 and 48, respectively, to keep the same power density. For the 330-MW(thermal) core, the void worth was reduced by 1.9% δk from the base core because the volume of the perturbed region is small in the spectral component of the void worth. The small core also has a greater leakage effect because the flux gradient is larger. Therefore, more fissile is charged to the core, and this changes the burnup reactivity swing to a positive value (0.4% δk) and reduces the minor actinide consumption. The effect of reactor power is summarized in Table IX.

TABLE IX

Effect of Reactor Power and Size

	Base	P600[a]	P330[b]
Power [MW(thermal)]	900	600	330
Cycle length (day)	304	304	304
Number of batches	2	2	2
Number of drivers	138	102	48
Actinide consumption (kg/yr)			
Fissile plutonium	−12	−8	−4
Total plutonium	−252	−169	−33
Minor actinide	531	355	136
Reactivity worth (BOEC)			
Burnup swing (% δk)	−2.1	−1.8	0.4
Void worth (% δk)	4.1	3.9	2.2
Doppler ($10^{-4}T\delta k/\delta T$)	−0.94	−0.93	−0.60

[a]Reactor power equals 600 MW(thermal).

[b]Reactor power equals 330 MW(thermal).

III.F. Effect of Core Geometry

III.F.1. Reduced Core Height

The core heights were reduced to 70.10 and 56.84 cm, which increased the number of drivers to 180 and 222, respectively, to maintain the same fuel volume. The characteristics of these cores are shown in Table X. The H/D ratio changed from 0.433 (base core) to 0.293 and 0.213 as the core height was reduced to 70.10 and 56.84 cm, respectively. Because of greater axial leakage in the smaller core (H = 56.84 cm), the charge enrichment was increased slightly, and the burnup reactivity swing was changed toward the positive direction. The consumption of minor actinides was reduced by 7% in the smaller core because their charge fraction was reduced by a similar rate. The void worth was reduced by 0.8%

TABLE X

Effect of Core Height

	Base	PAN70[a]	PAN57[b]
Power [MW(thermal)]	900	900	900
Cycle length (day)	304	304	304
Number of batches	2	2	2
Number of drivers	138	180	222
Core height (cm)	91.44	70.10	56.84
H/D ratio	0.433	0.293	0.213
Actinide consumption (kg/yr)			
Fissile plutonium	−12	−13	−14
Total plutonium	−252	−239	−213
Minor actinide	531	518	492
Reactivity worth (BOEC)			
Burnup swing (% δk)	−2.1	−1.9	−1.5
Void worth (% δk)	4.1	3.8	3.3
Doppler ($10^{-4}T\delta k/\delta T$)	−0.94	−1.06	−1.13

[a]Core height equals 70.1 cm, pancake-type core.
[b]Core height equals 56.84 cm, pancake-type core.

δk for the smaller core because the flux gradient is larger on the top and bottom boundaries, causing more neutron leakage, but the absolute value was still high (3.3% δk) and positive.

III.F.2. Annular Core Model

For a fixed fuel volume, the neutron leakage increases as the core surface area increases. The annular core was modeled by deploying several B_4C blocks in the central zone (Fig. 9), which increases the surface area of both the inner and outer boundaries. The power peak in the central zone could also be avoided with this geometry. Both the inner and outer boundaries are reflected with stainless steel blocks and shielded with B_4C blocks. Three different models were studied, as shown in Table XI.

The first model has the same number of drivers (138) as the base core, and the control rods are all withdrawn like the base core. So, the control rod sites are filled with sodium and duct material. Because of the increased leakage, the fissile charge was increased by 89% from the base core. Though this reduced the minor actinide consumption somewhat (~5%), the burnup reactivity swing and void worth were reduced to −1.6 and 3.6% δk, respectively. It was found that the peaking factor was changed from 1.55 to 1.46 as the model changed from the homogeneous base core to the annular core.

In the second model, the sodium of the control rod sites was replaced with HT-9 rods, which have the same size as a B_4C control rod. In other words, the HT-9 rods are used as a parking portion of the control rod, and therefore, the control sites are filled with HT-9 rods where the control rods are withdrawn. The neutron spectrum was not softened much because the HT-9 rods were sparsely distributed. Compared to the first model, the variations of performance parameters are small, i.e., ~4 and 7% reduction in minor actinide consumption and void worth, respectively.

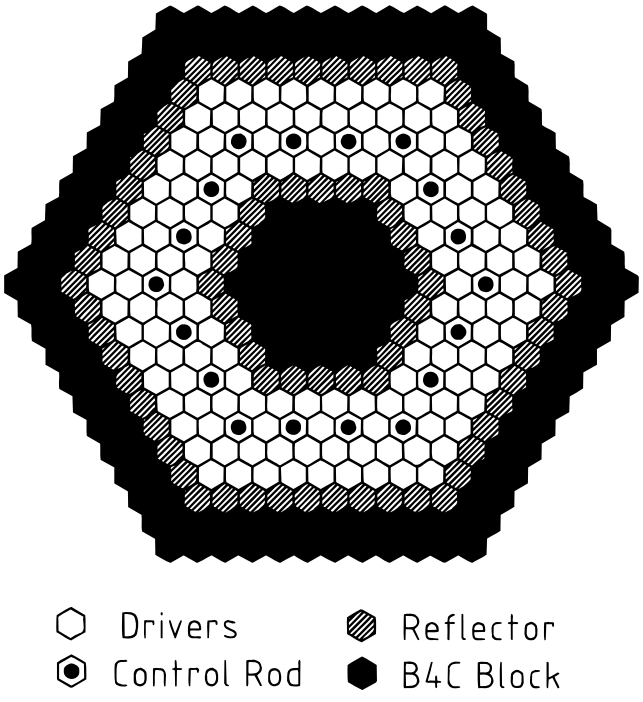

Fig. 9. Annular core model.

TABLE XI

Effect of Annular Geometry

	ANN1[a]	ANN2[b]	ANN3[c]
Power [MW(thermal)]	900	900	900
Cycle length (day)	304	304	304
Number of batches	2	3	3
Number of drivers	138	138	378
Fuel rods per assembly	271	271	91
Control rod site	Sodium	HT-9	HT-9
Actinide consumption (kg/yr)			
Fissile plutonium	−13	−14	124
Total plutonium	−222	−205	172
Minor actinide	502	484	118
Reactivity worth (BOEC)			
Burnup swing (% δk)	−1.6	−1.4	3.1
Void worth (% δk)	3.6	3.4	1.8
Doppler ($10^{-4} T\delta k/\delta T$)	−1.0	−1.0	−4.6

[a]Number of drivers equals 138, moderated by sodium, annular-type core.
[b]Number of drivers equals 138, moderated by HT-9, annular-type core.
[c]Number of drivers equals 378, moderated by HT-9, annular-type core.

In the last model, the sodium fraction of the driver was increased to 0.73, which is equivalent to an assembly with 91 regular fuel pins. The number of drivers was increased to 378, and the control rod sites were filled with HT-9 rods again. As in Sec. III.C, the softened spectrum caused more fissile loading and a deterioration of the minor actinide consumption.

III.G. Summary

Through the parametric study of homogeneous core models, it was found that the improvement in one performance parameter has drawbacks for other parameters. The minor actinide consumption depends on the amount of minor actinide material charged to the core, which is determined by the neutron spectrum and leakage rate. The sodium fraction and scattering material have a considerable effect on the neutron spectrum. The neutron leakage depends on the core geometry and the sodium fraction in the fuel assembly. The minor actinide consumption significantly deteriorates when the neutron spectrum is thermalized.

The reactivity burnup swing changes from negative to positive as the fissile enrichment increases. Though a zero burnup swing is achievable without hurting the peak linear power, the void worth is still high, and the minor actinide consumption is reduced because the minor actinide charge is decreased to accommodate ^{238}Pu buildup, which is highly reactive in the MAB studied here.

In most cases, the void worth is $>2\%$ δk. A negative void worth was obtained when the sodium fraction was large (0.73) and the power density was high, such as with a small core (222-driver core). Because the leakage becomes high in this core, the burnup reactivity swing and the minor actinide consumption deteriorate. A small void worth is achievable using scattering material, which prevents spectrum hardening to a certain extent, but the burnup reactivity swing and the minor actinide consumption are further reduced.

Compared to the pancake-type core, the annular core model has an advantage in reducing the power peaking without significantly deteriorating the burnup reactivity swing and the minor actinide consumption. Further void worth reduction is achievable by deploying scattering material (e.g., HT-9) in the control rod sites.

IV. DECOUPLED MINOR ACTINIDE BURNER DESIGN

The homogeneous core models have difficulty in simultaneously satisfying the MAB performance requirements of a massive minor actinide consumption rate, a low burnup reactivity swing, and a low void worth. In this section, results are reported for modeling the core with two different zones (decoupled core): a minor actinide zone and a plutonium-enriched zone. The minor actinide zone was used to burn the minor actinides effectively using a hard spectrum, while the plutonium zone was introduced to compensate for the deteriorating safety performance due to heavy minor actinide loading.

The decoupled core was modeled in annular geometry with HT-9 rods in control rod sites to prevent further spectrum hardening in the case of coolant voiding. After trying several models, a decoupled core was selected as the base model. In Secs. IV.A, IV.B, and IV.C, the property of the base core is discussed. A comparative study is done for the cores that have different characteristics.

IV.A. Base Decoupled Core

The base decoupled core has the same power [900 MW(thermal)] and core height (91.44 cm) as the homogeneous base core. The fuel cycle length is the same (304 days), but the number of batches was increased to three to increase the discharge burnup. There are 114 driver assemblies in both the inner and outer core zones. The sodium fractions of the inner and outer core assemblies are 0.36 and 0.73, respectively, which correspond to 271 and 91 regular fuel pins per assembly, respectively. The sodium fraction in the outer core is larger to cause more neutron leakage. The minor actinide and plutonium fuels are loaded in the inner and outer core zones, respectively. The characteristics and configuration of the base decoupled core are shown in Table XII and Fig. 10, respectively. The compositions of the inner and outer core fuel are given in Table XIII.

Compared to the results of the homogeneous base core, both the burnup reactivity swing and the void worth were improved in the decoupled core, but the minor actinide consumption was decreased by 189 kg/yr. The burnup reactivity swing became relatively small (1.04% δk) because the ^{238}Pu buildup from the neutron capture of ^{237}Np was compensated for by the fissile (^{239}Pu and ^{241}Pu) burning in the outer core. The sodium void worth was reduced to 1.2% δk at the BOEC state. Spectrum hardening caused more neutron production in the inner core, but the production rate in the outer core decreased more than the absorption rate because the total flux level decreased to compensate for the power increase in the inner core. Therefore, it was possible to achieve a smaller void worth in the decoupled core.

TABLE XII

Characteristics of Decoupled Base Core

Reactor concept	Decoupled annular
Reactor power [MW(thermal)]	900
Active core height (cm)	91.44
Breeding ratio	0.15
Number of drivers	
Inner core	114
Outer core	114
Fuel pins per assembly	
Inner core	271
Outer core	91
Fuel mass ratio	
Inner core (U/Np/Am/Cm)	5/75/12/8
Outer core (Np/Pu/Cm)	7/92/1
Discharge burnup (MWd/kg)	
Inner core	64
Outer core	173
Actinide consumption (kg/yr)	
Fissile plutonium	121
Total plutonium	−55
Minor actinide	342
Burnup swing (% δk)	1.04
Void worth (% δk)	
BOEC	1.16
EOEC	1.51
Doppler ($10^{-4} T\delta k/\delta T$)	
BOEC	−3.19
EOEC	−3.15

IV.B. Effect of Moderating Material

The outer core driver of the base decoupled core was changed to have 78 and 180 BeO rods in the medium-moderated and highly moderated cores, respectively, to soften the spectrum in this region. The moderating pin has the same size as the regular fuel pin. Therefore, the sodium coolant area of the highly moderated core is the same in both the inner and outer core assemblies because there are 91 plutonium fuel pins of regular size. The core configuration is the same as the base decoupled core.

As the number of moderating pins increased, the burnup reactivity swing increased because more fissile plutonium was consumed by fission and parasitic capture. The void worth was reduced by the use of moderating pins, which somewhat prevent spectrum hardening upon coolant voiding. The Doppler constant increased also in magnitude because the spectrum shifted toward the resolved resonance region where the Doppler effect was dominant.

For the highly moderated core, the burnup reactivity swing increased to 3.7% δk. The minor actinide consumption was reduced by 59 kg/yr compared to the base decoupled core. The void worth was reduced to 0.47% δk at the BOEC state, but the linear power of the outer core fuel pin was increased to 70 kW/m. The characteristics of the moderated core are shown in Table XIV. Though the moderated core has an advantage in the void worth, it is doubtful that the moderated core would be attractive because of the large burnup reactivity swing and high linear power.

IV.C. Effect of Outer Core Size

The number of assemblies in the outer core was increased from 114 (base decoupled core model) to 138 and 210 in the medium and large cores, respectively. There

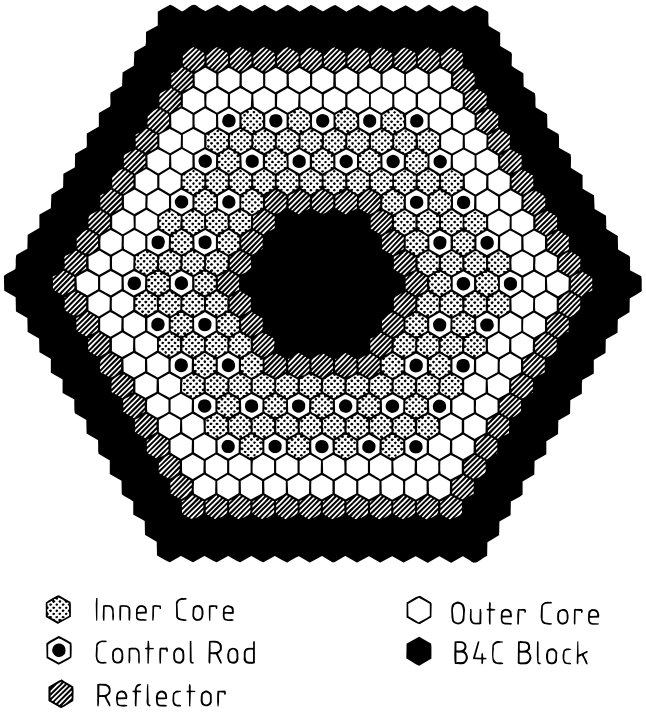

Fig. 10. Decoupled base core model.

are 66 control rod sites in both the medium and large cores, while the base decoupled core has 42 control rod sites that are filled with the HT-9 rods. As the outer core size increased, the burnup reactivity swing increased. More fissile plutonium was transmuted in the outer core, but the minor actinide consumption was decreased because the power level was reduced in the inner core. The minor actinide consumption was decreased by 28 and 36 kg/yr for the medium and large cores, respectively, compared to the base decoupled core.

The void worth was smaller in the medium core (1.05% δk at EOEC), while it was larger (1.62% δk at EOEC) for the large core. The Doppler constants were not much different in each core model. The medium core showed the better performance in the void worth though the burnup reactivity swing and the minor actinide consumption were slightly reduced. In the medium core, the peak linear power of the inner core pin had sufficient margin, and the discharge burnup was still below the design limit (200 MWd/kg). Therefore, it was decided to elevate the reactor power in the final core model such that the minor actinide consumption could be increased and to use a smaller fuel pin in the outer core to prevent a large temperature rise in the pin. The properties of these cores are compared in Table XV.

TABLE XIII

Fuel Composition of Decoupled Base Core

Isotope	Inner Core		Outer Core	
	Atom Density (10^{24} cm^{-3})	Fraction (%)	Atom Density (10^{24} cm^{-3})	Fraction (%)
^{234}U	2.3276E−04[a]	3.08	9.2196E−06	0.36
^{235}U	4.5884E−05	0.61	1.6718E−06	0.07
^{236}U	3.6302E−05	0.48	1.3370E−06	0.05
^{238}U	3.1716E−08	0.00	1.2380E−09	0.00
^{237}Np	5.6839E−03	75.17	1.6948E−04	6.68
^{236}Pu	0.0000E+00	0.00	4.6719E−09	0.00
^{238}Pu	2.2506E−07	0.00	2.0889E−04	8.23
^{239}Pu	7.5849E−08	0.00	1.1958E−03	47.13
^{240}Pu	8.3310E−06	0.11	5.2813E−04	20.81
^{241}Pu	4.7635E−09	0.00	2.9405E−04	11.59
^{242}Pu	5.3103E−09	0.00	1.0258E−04	4.04
^{241}Am	4.7202E−04	6.24	7.6136E−06	0.30
^{242m}Am	2.4800E−06	0.03	1.6950E−08	0.00
^{243}Am	4.6590E−04	6.16	5.6975E−07	0.02
^{242}Cm	1.9419E−07	0.00	3.9783E−09	0.00
^{243}Cm	4.4281E−06	0.06	1.0886E−07	0.00
^{244}Cm	4.3143E−04	5.71	1.2013E−05	0.47
^{245}Cm	1.1793E−04	1.56	3.9201E−06	0.15
^{246}Cm	5.9245E−05	0.78	2.0951E−06	0.08

[a]Read as 2.3276×10^{-4}.

TABLE XIV

Effect of Moderating Pins in Outer Core

	Base	M78[a]	M180[b]
Power [MW(thermal)]	900	900	900
Cycle length (day)	304	304	304
Number of batches	3	3	3
Number of drivers			
Inner core	114	114	114
Outer Core	114	114	114
BeO pins per outer core assembly	0	78	180
Actinide consumption (kg/yr)			
Fissile plutonium	135	139	168
Total plutonium	−41	−37	1
Minor actinide	342	323	283
Burnup swing (% δk)	1.04	1.82	3.67
Void worth (% δk)			
BOEC	1.16	1.00	0.47
EOEC	1.51	1.55	1.23
Doppler ($10^{-3}T\delta k/\delta T$)			
BOEC	−0.32	−0.70	−2.08
EOEC	−0.32	−0.63	−1.75

[a]Number of BeO pins per outer core assembly equals 78.
[b]Number of BeO pins per outer core assembly equals 180.

TABLE XV

Effect of Outer Core Size

	Base	O138[a]	O210[b]
Power [MW(thermal)]	900	900	900
Cycle length (day)	304	304	304
Number of batches	3	3	3
Number of drivers			
Inner core	114	114	114
Outer core	114	138	210
Number of control rods	42	66	66
Actinide consumption (kg/yr)			
Fissile plutonium	135	140	147
Total plutonium	−41	−26	−18
Minor actinide	342	314	306
Burnup swing (% δk)	1.04	1.40	1.61
Void worth (% δk)			
BOEC	1.16	0.72	1.18
EOEC	1.51	1.05	1.62
Doppler ($10^{-3}T\delta k/\delta T$)			
BOEC	−0.32	−0.34	−0.31
EOEC	−0.32	−0.33	−0.31

[a]Number of drivers in outer core equals 138.
[b]Number of drivers in outer core equals 210.

V. FINAL CORE MODEL

The final core consists of 114 inner core assemblies (minor actinide fuel), 138 outer core assemblies (plutonium fuel), and 66 control rod sites (same as the medium-core model in Sec. IV.C). But, the reactor power was set at 1200 MW(thermal) to increase the minor actinide consumption. Both the inner and outer boundaries are surrounded with stainless steel reflector and shielded with B_4C blocks. The control rod sites are filled with HT-9 rods when control rods are not inserted in order to reduce the spectrum hardening in the event of coolant voiding. The upper and lower plenum regions are composed of HT-9 structural material and sodium coolant. The upper and lower shields are placed next to the plenum region. The thickness of the plenum and shield are the same as those of the homogeneous base core model. The horizontal and vertical configurations of the core are shown in Figs. 11 and 12, respectively.

The minor actinide and plutonium fuel assemblies have 271 and 162 fuel pins, respectively. The fuel has 25% zirconium, and the theoretical density was assumed to be 75% to allow for fuel expansion and high discharge burnup. The isotopic compositions of the inner and outer core assemblies were determined using the equilibrium cycle capability of the REBUS-3 code. The inner core fuel is composed of 70% ^{237}Np, and the outer core fuel is enriched to 50% with fissile plutonium. The plutonium fuel pin diameter is smaller to reduce the fuel center temperature. Because the outer core fuel is highly enriched and the inner core contains fertile ^{237}Np, the power shifts from the outer to the inner core during the cycle. The general core characteristics and fuel assembly data are summarized in Tables XVI and XVII, and the fuel

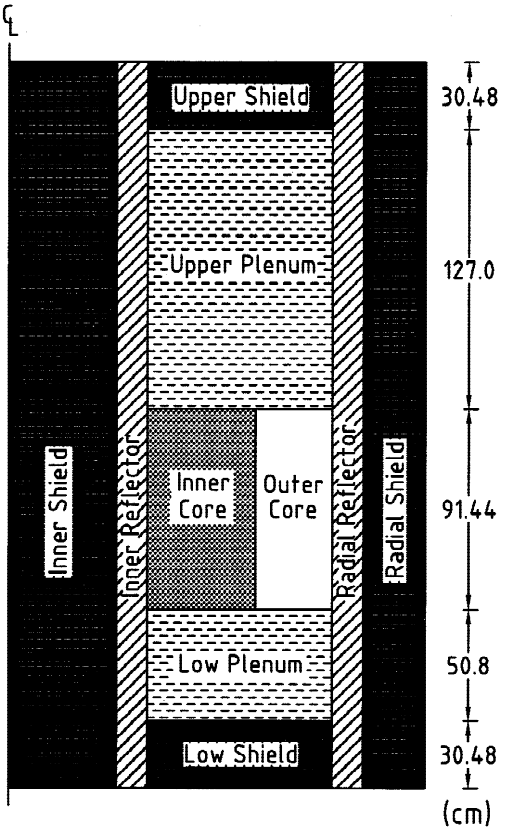

Fig. 12. Vertical view of final MAB model.

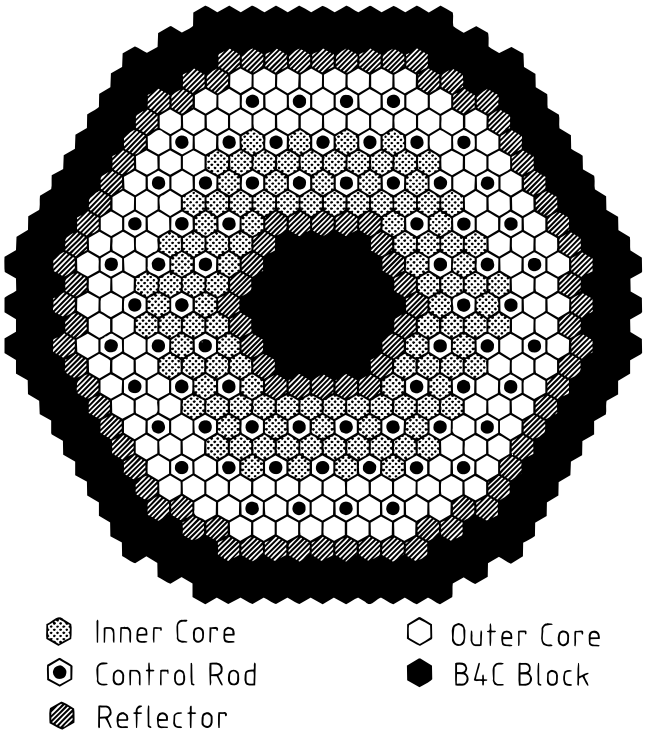

Fig. 11. Horizontal view of final MAB model.

TABLE XVI

General Specifications of Final MAB Model

Core concept	Decoupled annular
Reactor power [MW(thermal)]	1200
Fuel height (cm)	91.44
Number of assemblies	
Inner core	114
Outer core	138
Number of control rods	66
Control rod parking material	HT-9
Structural material	HT-9
Capacity factor (%)	80
Cycle length (day)	304
Fuel residence time (cycles)	3

TABLE XVII

Fuel Assembly Data of Final MAB Model

	Inner Core	Outer Core
Fuel type	U/Np/Am/Cm + 25% Zr	U/Np/Pu/Cm + 25% Zr
Mass ratio (U/Np/Pu/Am/Cm)	5/71/0/15/9	1/8/90/0/1
Volume ratio (Fuel/coolant/structure)	38/36/26	13/72/15
Number of pins per assembly	271	162
Fuel pin diameter (cm)	0.724	0.544
Cladding thickness (cm)	0.056	0.043
Pitch-to-diameter ratio	1.18	1.96
Fuel smear density (% theoretical density)	75	75
Assembly lattice pitch (cm)	15.4686	15.4686

composition is shown in Table XVIII. The equilibrium cycle performance parameters are given in Table XIX.

V.A. Fuel Cycle

The MAB is operated with three fuel batches and a 10-month cycle length. The relatively short cycle length is used to maintain an acceptable burnup reactivity swing. The feed material for the MAB is assumed to be from a typical 1000-MW(electric) LWR after 3 yr cooling. At the completion of each burnup cycle, the discharged fuel is recovered and fabricated with external feed material in the fabrication plant. The external feed material is assumed to be provided as separate plutonium and minor actinide streams, with the isotopic distributions shown in Table II.

TABLE XVIII

Fuel Composition of Final MAB Model

	Inner Core		Outer Core	
Isotope	Atom Density (10^{24} cm^{-3})	Fraction (%)	Atom Density (10^{24} cm^{-3})	Fraction (%)
^{234}U	2.7395E−04[a]	3.63	1.4224E−05	0.56
^{235}U	5.3394E−05	0.71	2.6069E−06	0.10
^{236}U	4.2162E−05	0.56	2.0733E−06	0.08
^{238}U	3.6006E−08	0.00	1.8415E−09	0.00
^{237}Np	5.3871E−03	71.40	2.0370E−04	8.02
^{236}Pu	0.0000E+00	0.00	3.9671E−09	0.00
^{238}Pu	1.7186E−07	0.00	2.3588E−04	9.28
^{239}Pu	8.2770E−08	0.00	1.1432E−03	44.98
^{240}Pu	8.8380E−06	0.12	5.2560E−04	20.68
^{241}Pu	4.9449E−09	0.00	2.7791E−04	10.94
^{242}Pu	5.6265E−09	0.00	1.0289E−04	4.05
^{241}Am	5.6880E−04	7.54	7.5428E−06	0.30
^{242m}Am	3.0582E−06	0.04	3.0581E−08	0.00
^{243}Am	5.6166E−04	7.44	8.7251E−07	0.03
^{242}Cm	1.4922E−07	0.00	2.3248E−09	0.00
^{243}Cm	4.6273E−06	0.06	1.4191E−07	0.01
^{244}Cm	4.5769E−04	6.07	1.6445E−05	0.65
^{245}Cm	1.2242E−04	1.62	5.3990E−06	0.21
^{246}Cm	6.0464E−05	0.80	2.8664E−06	0.11

[a]Read as 2.7395×10^{-4}.

TABLE XIX

Equilibrium Cycle Performance Parameter of Final MAB Model

	Inner Core	Outer Core
Power fraction (%)		
BOEC	45.64	52.31
EOEC	54.18	43.77
Peak linear power (kW/m)		
BOEC	33.3	40.3
EOEC	33.9	34.0
Power peaking factor		
BOEC	1.72	1.31
EOEC	1.47	1.32
Peak flux (10^{15}/cm^2·s)		
BOEC	3.33	3.43
EOEC	3.33	3.36
Breeding ratio	0.03	0.12
Discharge burnup (MWd/kg)	82.08	198.70

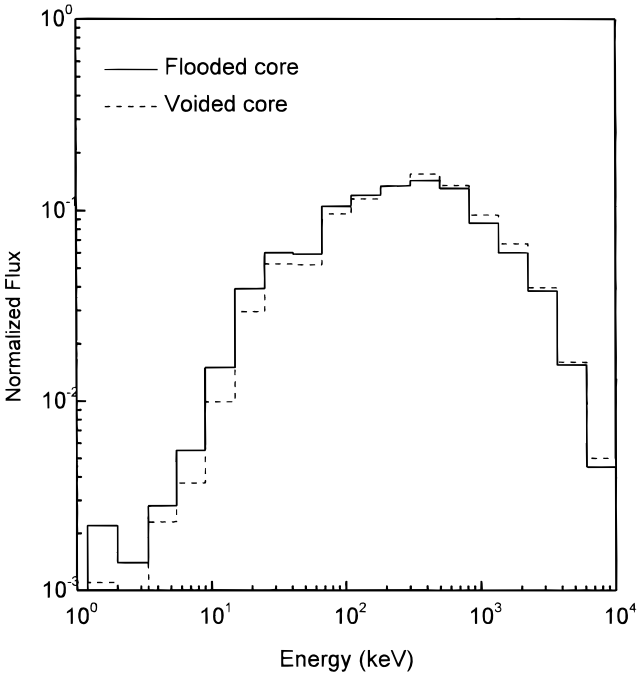

Fig. 13. Spectrum hardening in inner core.

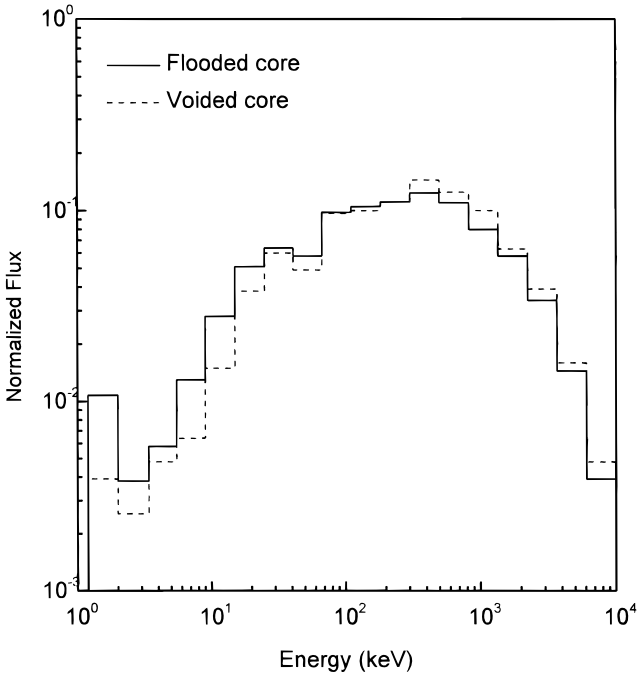

Fig. 14. Spectrum hardening in outer core.

The MAB accepts 694 kg/yr of minor actinides and 552 kg/yr of plutonium. The minor actinides are continuously recycled in the core; however, 70% of the fissile plutonium is surplus material and is assumed to be used as fissile makeup in other plutonium-burning reactors. Considering 96% of the discharged americium is not recovered in the reprocessing plant, the net consumption rate of minor actinides is 426 kg/yr. Assuming the typical 1000-MW(electric) LWR generates ~26 kg of minor actinides each year, the core design here can consume the annual minor actinide inventory from about 16 LWRs.

V.B. Safety Performance Parameters

The reactivity of the inner core will increase substantially with burnup since the minor actinide fuel consists mostly of ^{237}Np ($\eta = 0.94$), which results in ^{238}Pu ($\eta = 2.46$) after neutron capture. As the fuel depletes, this reactivity gain is compensated for by the decrease in the fissile plutonium inventory in the outer core, resulting in a small positive burnup reactivity swing (1.19% δk).

The dominant contribution to the sodium void worth is spectral hardening (Figs. 13 and 14), which is mitigated to some extent by using the HT-9 rods in the control rod sites. The isotope most responsible for the increase in reactivity upon coolant voiding is ^{237}Np, for which η changes from 0.94 to 1.09 as the coolant voids in the inner core where the neutron mean energy changes from 625 to 670 keV. However, as the coolant voids in the outer core, the neutron leakage increases because the neutron mean energy increases from 594 to 667 keV (spectrum hardening) and the neutron mean free path increases. Spectral hardening causes a power reduction in the outer core while it increases the power in the inner core because of increased fast fission. Because the outer core is predominantly fissile material, a decrease in the power reduces the neutron production rate more than the

absorption rate, which provides a negative coolant void worth in this region. Because the positive reactivity effect of the inner core dominates, the net effect is still a small positive void worth; however, it is comparable to void worths allowed in conventional LMR designs.

Because the actinide burner does not contain ^{238}U, the Doppler effect is smaller than in a conventional LMR but remains negative ($-0.35 \times 10^{-3} T\delta k/\delta T$). At the EOEC, the core contains ~50% ^{237}Np, and therefore, the largest contribution to the Doppler effect is from ^{237}Np even though its highest resolved resonance is at 130 eV. The ^{240}Pu and ^{242}Pu have their strong resolved resonances at ~2.4 and 0.9 keV, respectively, but their contribution to the Doppler reactivity is small since they comprise only 6.8 and 1.4% of the EOEC loading, respectively. The safety performance parameters are summarized in Table XX for both the BOEC and the EOEC core conditions.

V.C. Estimation of Fuel Temperature

The ultimate safety of the reactor core is the fuel integrity in the case of TOP. Though the material and thermal properties of the minor actinide and plutonium fuel are not yet known, it is worthwhile to estimate the fuel temperature using currently available or assumed data because the fuel temperature must not exceed the melting point. The thermal conductivity of the fuel is assumed to be 22 W/m·K based on SAFR and Japanese ABR designs. The specific heat and velocity of sodium coolant are 1.3 kJ/kg·°C and 6 m/s, respectively, based on Ref. 27 and ABR design. The bulk coolant temperature is assumed to be 650 K. The sodium density and thermal conductivity are obtained using the following relations:

$$\rho_l\,(\mathrm{kg/m^3}) = 1011.8 - 0.22054T - 1.9226 \times 10^{-5}T^2 + 5.6371 \times 10^{-9}T^3 \qquad (4)$$

and

$$k\,(\mathrm{W/m\cdot K}) = 93.0 - 0.0581(T - 273) + 1.173 \times 10^{-5}(T - 273)^2\ , \qquad (5)$$

where T is temperature in kelvins. The cladding temperature was assumed to be 750 K for the initial calculation. The thermal conductivity of the clad material was obtained using the relation of Type 316 stainless steel as follows:

$$k\,(\mathrm{W/m\cdot K}) = 9.248 + 0.01571T\ , \qquad (6)$$

where T is temperature in kelvins. The calculated and assumed thermal properties are summarized in Table XXI.

TABLE XX

Safety Performance Parameters of Final MAB Model

	BOEC	EOEC
Burnup swing (% δk)	1.19	
Void worth (% δk)	0.74	1.17
Doppler ($10^{-3} T\delta k/\delta T$)	−0.35	−0.32

V.C.1. Inner Core Fuel Pin

The inner core assembly has 271 regular fuel pins, of which the outer diameter, clad thickness, and pin pitch are 0.724, 0.056, and 0.853 cm, respectively. Using these values, the P/D, flow area A, wetted perimeter Pw, and effective hydraulic diameter De of a subchannel were calculated, which are 1.18, 0.1098 cm^2, 1.1379 cm, and 0.3855 cm, respectively. Then, the Peclet number Pe was calculated to be 356, and the Nusselt number Nu was obtained as 7.53 using the Borishanskii-Gotovskii-Firsova (B-G-F) correlation,[33] which is applicable for $1.1 \le P/D \le 1.5$ and $200 \le \mathrm{Pe} \le 2000$. Finally, the heat transfer coefficient was calculated from another formulation for the Nusselt number:

$$h = \mathrm{Nu}\,\frac{k}{De} = 142\,000\ \mathrm{W/m^2\cdot K}\ . \qquad (7)$$

The position of the maximum fuel-center temperature along the fuel element is obtained using the equations in Ref. 34. The maximum coolant temperature rise was 24 K, and therefore, the maximum coolant temperature at the peak position was 654 K when the inlet temperature was 630 K. The temperature rise between the bulk coolant and the fuel center was 225 K, which resulted in a fuel-center temperature of 879 K (606°C). If there is 115% overpower, the coolant temperature rise will be 28 K, and the maximum coolant temperature is 658 K. Then, the fuel-center temperature will be 917 K (644°C), which is considerably below the melting point (1160°C).

TABLE XXI

Thermal Property Data

Fuel thermal conductivity (W/m·K)	22
Clad thermal conductivity (W/m·K)[a]	21
Coolant	
Inlet temperature (K)	630
Bulk temperature (K)	650
Density (kg/m^3)	862
Thermal conductivity (W/m·K)	73
Specific heat (kJ/kg·°C)	1.3
Velocity (m/s)	6

[a]At 750 K.

V.C.2. Outer Core Fuel Pin

The final core model has 162 fuel pins in an outer core assembly with reduced pin size. For comparison, the fuel temperature was calculated for three different numbers of fuel pins: 91, 127, and 162, of which the pin sizes are 0.724, 0.612, and 0.544 cm. Therefore, the material volumes of fuel, clad, and coolant are conserved in the three models such that the neutronic calculation will not be affected. The Graber and Rieger correlation[27] was used to determine the Nusselt number for the range of $1.25 \leq P/D \leq 1.95$ and $150 \leq \text{Pe} \leq 3000$. The fuel temperatures are listed in Table XXII with other parameters. For the assembly with 162 fuel pins, the centerline temperature was 640°C. In the case of 115% overpower transient, the fuel temperature increased to 683°C, and there was still a 41% margin for fuel melting.

V.D. Summary

An MAB was designed using several parametric studies. For the homogeneous core models, the void worth became unacceptably large (positive) as the minor actinide inventory was increased because of the fast fission effect of the minor actinides (e.g., ^{237}Np). On the other hand, if the fuel volume fraction was reduced to increase the core leakage and reduce the void worth, the reactivity burnup swing became unacceptably large, and the minor actinide inventory was reduced.

One of the principal innovations used in the conceptual MAB design is to maintain a homogeneous core layout but employ two core zones: an inner core consisting of minor actinide fuel and an outer core containing plutonium fuel. The plutonium outer core offsets much of the poor safety performance of the core, caused by the presence of minor actinides in the inner core. The HT-9 rods are employed in the control rod sites as a means of further reducing the sodium void worth.

The final MAB model can consume the annual minor actinide waste from about 16 commercial LWRs. Because of the decoupled core design innovation, it was possible to maintain acceptable safety performance as indicated by the small burnup reactivity swing, the low sodium void worth, and the negative Doppler constant. The fuel temperature was also kept below the melting point both in the inner and outer cores.

VI. SUMMARY, CONCLUSIONS, AND RECOMMENDATIONS

The feasibility of using minor actinides as fuel material in an LMR to reduce the long-term hazard due to the minor actinides discharged from an LWR was studied in the work here. The principal problem of designing a minor actinide burning reactor is the difficulty in maintaining a small burnup reactivity swing and void worth while maximizing the minor actinide consumption rate. In the case of a homogeneous core model, it was found that the burnup reactivity swing becomes large when the void worth is reduced because of a large increase in the neutron leakage. The minor actinide consumption rate also deteriorates because the core is primarily charged with fissile material to compensate for the reactivity loss due to the increased neutron leakage.

TABLE XXII

Effect of Outer Core Pin Size in Final MAB Model

Parameter	Fuel Pins per Assembly		
	91	127	162
Outer diameter (cm)	0.724	0.612	0.544
Clad thickness (cm)	0.056	0.048	0.043
Pin pitch (cm)	1.524	1.219	1.067
P/D	2.100	1.992	1.963
A (cm^2)	0.813	0.497	0.374
Pw (cm)	1.138	0.963	0.853
De (m)	0.029	0.021	0.018
$\dot{m}$ (kg/s)	0.420	0.257	0.194
Pe	2 671	1 906	1 631
Nu	261	197	175
h (W/m$^2\cdot$K)	657 000	685 000	710 000
$\Delta T_{coolant}$ (K)	58.7	86.9	81.8
ΔT_{fuel} (K)	357	257	202
$T_{fuel\text{-}center}$ (K)	1 046	974	913

A conceptual design of the MAB was performed using several parametric studies to maximize the consumption of minor actinides discharged from the LWR. The design effort was focused on reducing the burnup reactivity swing and coolant void worth while keeping the Doppler constant negative. The core was designed in an annular decoupled model in which the minor actinides were transmuted in the inner core surrounded by the plutonium outer core to compensate for the deleterious effect of the minor actinides on the core safety performance.

The reactivity increases in the inner core zone during the cycle because the neutron capture of ^{237}Np produces ^{238}Pu, which is more reactive in the MAB. The reactivity gain in the inner core is compensated for by fissile burning in the outer core. Because the reactivity loss is higher in the outer core, the burnup reactivity swing is positive and small (1.19% δk).

The void worth becomes positive and large in the inner core because the minor actinides such as ^{237}Np undergo more fast fission (i.e., η increases) when the neutron spectrum is hardened. Because of the increased fast fission in the inner core, the power level in the outer core is reduced. Because of the nuclear properties of the fissile material loaded in the outer core, the production rate is reduced considerably in the outer core, resulting in a small void worth for the entire core (1.17% δk at EOEC).

The Doppler constant was very small (-0.35×10^{-3} $T\delta k/\delta T$) because the fertile material such as ^{238}U was not supplied from an external source to prevent further minor actinide production. By adopting the annular decoupled core model, it was possible to consume 426 kg/yr of minor actinides, which is equivalent to the minor actinides discharged from sixteen 1000-MW(electric) LWRs.

As a recommendation, more research is required in the following areas:

1. The feasibility of minor actinide burning is strongly dependent on the demonstration of fuel reprocessing and refabrication techniques. This should be a high priority for minor actinide burning research.

2. The disposition of the excess plutonium produced from the MAB was not considered in this work. Though the plutonium can be used in several reactor types, it would be worthwhile to perform a detailed study in conjunction with MAB research.

3. A harder neutron spectrum is especially beneficial for burning minor actinides and would improve the void coefficient. It would be worthwhile to investigate the neutronics and mechanical feasibility of using lead as a coolant.

ACKNOWLEDGMENTS

This work was sponsored by the U.S. Department of Energy under contract FG07-88ER12812, and the publication was carried out under the Nuclear Research and Development program of the Korea Ministry of Science and Technology.

REFERENCES

1. H. C. CLAIBORNE, "Neutron-Induced Transmutation of High-Level Radioactive Waste," ORNL-TM-3964, Oak Ridge National Laboratory (1972).

2. A. S. KUBO and D. J. ROSE, "Disposal of Nuclear Waste," *Science*, **182**, 1205 (1973).

3. J. W. BARTLETT et al., "High-Level Radioactive Waste Management Alternatives, Section 7: Waste Partitioning," BNWL-1900, Battelle Pacific Northwest Laboratories (1974).

4. R. J. BREEN, "Elimination of Actinides with LMFBR Recycle," *Trans. Am. Nucl. Soc.*, **21**, 262 (1975).

5. T. H. PIGFORD and J. S. CHOI, "Actinide Transmutation in Fission Reactors," *Trans. Am. Nucl. Soc.*, **27**, 450 (1977).

6. A. G. CROFF, "Parametric Studies Concerning Actinide Transmutation in Power Reactors," *Trans. Am. Nucl. Soc.*, **22**, 345 (1975).

7. S. L. BEAMAN, "Actinide Recycle in LMFBRs as a Waste Management Alternative," *Trans. Am. Nucl. Soc.*, **22**, 346 (1975).

8. M. L. WILLIAMS et al., "Preliminary Neutronic Study of Actinide Transmutation in a Fast Reactor," ORNL/TM-6309, Oak Ridge National Laboratory (1978).

9. J. J. PRABULOS, "Actinide Destruction in a 1500 MW(e) Carbide-Fueled LMFBR," *Trans. Am. Nucl. Soc.*, **23**, 548 (1976).

10. S. L. BEAMAN and E. A. AITKEN, "Feasibility Studies of Actinide Recycle in LMFBRs as a Waste Management Alternative," *Trans. Am. Nucl. Soc.*, **23**, 547 (1976).

11. A. H. ROBINSON et al., "Burning Actinides in Very Hard Spectrum Reactors," *Trans. Am. Nucl. Soc.*, **30**, 289 (1978).

12. W. BALZ et al., "Core Design and Safety Aspects of Large LMFBRs with Minor Actinide Recycling," *Proc. Int. Fast Reactor Safety Mtg.*, Snowbird, Utah, August 12–16, 1990, Vol. I, p. 153, American Nuclear Society (1990).

13. T. WAKABAYASHI et al., "Status of Study on TRU Transmutation in LMFBRs," *Trans. Am. Nucl. Soc.*, **64**, 556 (1991).

14. T. HAYASE et al., "Core Design Study for Actinide Burning LMFBRs," *Proc. Int. Conf. Physics of Reactor Operation, Design and Computation*, Marseille, France, April 23–26, 1990, Vol. 4 (1990).

15. T. MUKAIYAMA et al., "Minor Actinide Transmutation in Minor Actinide Burner Reactors," *Trans. Am. Nucl. Soc.*, **64**, 548 (1991).

16. A. SASAHARA and T. MATSUMURA, "An Assessment of TRU Recycling Transmutation in Metal Fuel FBR," *Proc. Int. Conf. Physics of Reactor Operation, Design and Computation*, Marseille, France, April 23–26, 1990.

17. R. N. HILL et al., "Physics Studies of Higher Actinide Consumption in an LMR," *Proc. Int. Conf. Physics of Reactor Operation, Design and Computation*, Marseille, France, April 23–26, 1990, Vol. 1 (1990).

18. D. C. WADE and Y. I. CHANG, "The Integral Fast Reactor Concept: Physics of Operation and Safety," *Nucl. Sci. Eng.*, **100**, 507 (1988).

19. ROCKWELL INTERNATIONAL, "Characteristics of a Minor Actinide Fueled Reactor," *Proc. Transmutation Workshop of the FFTF Internationalization Symp.*, WHC-MR-0262, Westinghouse Hanford Company (1991).

20. Y. ORECHWA et al., "Core Design and Performance of Small Inherently Safe LMRs," *Proc. Topl. Mtg. Advances in Fuel Management*, Pinehurst, North Carolina, March 2–5, 1986, p. 152, American Nuclear Society (1986).

21. T. MUKAIYAMA, "Actinide Burner Reactor for Minor Actinide Transmutation: Design Study and Integral Experiment for Nuclear Fuel Material Evaluation," *Proc. Transmutation Workshop of the FFTF Internationalization Symp.*, WHC-MR-0262, Westinghouse Hanford Company (1991).

22. K. L. DERSTINE, "DIF3D: A Code to Solve One-, Two-, Three-Dimensional Finite-Difference Diffusion Theory Problems," ANL-82-64, Argonne National Laboratory (1984).

23. B. TOPPEL, "A Users' Guide for the REBUS-3 Fuel Cycle Analysis Capability," ANL-83-2, Argonne National Laboratory (1983).

24. L. BURRIS et al., "A Proposed Pyrometallurgical Process for Rapid Recycle of Discharged Fuel Materials from the Integral Fast Reactor," *Proc. Topl. Mtg. Fuel Reprocessing and Waste Management*, Jackson, Wyoming, August 26–29, 1984, Vol. II, p. 2-257, American Nuclear Society (1984).

25. R. N. HILL, "Physics Studies of Higher Actinide Consumption in an LMR," Intra-Laboratory Memo., Applied Physics Division, Argonne National Laboratory (September 2, 1988).

26. T. HAMID, "Study of a New Compact Fast Reactor Core Design," PhD Thesis, School of Nuclear Engineering, Purdue University (1990).

27. A. E. WALTAR and A. B. REYNOLDS, *Fast Breeder Reactors*, Pergamon Press, New York (1981).

28. "Decrease of Sodium Void Reactivity of Large Mox FBR Cores," presented at Argonne National Laboratory, FN-ENZ-528, Hitachi, Ltd. (1991).

29. R. N. HILL et al., "Calculational Benchmark Comparisons for a Low Sodium Void Worth Actinide Burner Core Design," *Proc. Topl. Mtg. Advances in Reactor Physics*, Charleston, South Carolina, March 8–11, 1992, Vol. 1, p. 1-313, American Nuclear Society (1992).

30. S. GLASSTONE and A. SESONSKE, *Nuclear Reactor Engineering*, Van Nostrand Reihold Company, New York (1981).

31. H. KUSTERS and H. W. WIESE, "Burning of Actinides and Fission Products in Reactors and Accelerator-Driven Spallation Sources," *Trans. Am. Nucl. Soc.*, **64**, 544 (1991).

32. H. S. KHALIL and R. N. HILL, "An Evaluation of Liquid Metal Reactor Design Options for Reduction of Sodium Void Worth," *Nucl. Sci. Eng.*, **109**, 221 (1991).

33. V. M. BORISHANSKII et al., "Heat Transfer to Liquid Metal Flowing Longitudinally in Wetted Bundles of Rods," *Sov. At. Energy*, **27**, 1347 (1969).

34. M. M. EL-WAKIL, *Nuclear Heat Transport*, International Textbook Company, Scranton, Pennsylvania (1971).